Size- and orientation-selective optical manipulation of single-walled carbon nanotubes: A theoretical study

Hiroshi Ajiki*
Photon Pioneers Center, Osaka University, 2-1 Yamadaoka, Suita, Osaka 565-0871, Japan

Takuya Iida
Nanoscience and Nanotechnology Research Center, Research Institutes for the Twenty-first Century, Osaka Prefecture University, 1-2 Gakuencho, Nakaku, Sakai, Osaka 599-8570, Japan and PRESTO, Japan Science and Technology Agency, 4-1-8 Honcho, Kawaguchi, Saitama 332-0012, Japan

Takahiro Ishikawa, Seiji Uryu, and Hajime Ishihara
Department of Physics and Electronics, Osaka Prefecture University, 1-1 Gakuencho, Nakaku, Sakai, Osaka 599-8531, Japan
(Received 11 May 2009; revised manuscript received 18 August 2009; published 30 September 2009)

We have theoretically studied the resonant radiation force exerted on single-walled carbon nanotubes (SWCNs) by taking into account the excitonic effect under the effective-mass approximation. When a light frequency is close to an exciton level, the radiation force becomes significantly large even at room temperature for conventional laser intensities in optical manipulation. The peak positions in radiation force spectra are sensitive to the tube diameter and light polarization. Furthermore, the chirality dependence on exciton for similar diameter is relatively large. Therefore, the selective sorting and trapping of SWCNs with a desired specific structure is possible by tuning the applied field frequency.

DOI: 10.1103/PhysRevB.80.115437 PACS number(s): 78.67.Ch, 71.35.Gg, 42.50.Wk

I. INTRODUCTION

A single-walled carbon nanotube (SWCN) has very attractive electronic, magnetic, and optical properties because of its unique quasi-one-dimensional structure.[1,2] For example, SWCNs are metals or semiconductors depending on the diameter and chirality.[3–6] Another typical example is the Aharonov-Bohm (AB) effect, where a band gap can be changed by applying a magnetic flux passing through the cross section.[6–8] As for mechanical properties, a carbon nanotube (CN), including a multiwalled CN, is lightweight and has high mechanical strength. Because of these characteristic properties, CNs have been widely studied in various research fields and are expected to have many applications as efficient electron emitters,[9] the probe tip of the scanning force microscope with extremely high spatial resolution,[10] thermal light-emitting devices with a specific wavelength depending on their diameter,[11] SWCN field-effect transistors with ballistic electronic transport,[12] biosensors with high sensitivity,[13] and so on.[14]

In order to study fundamental properties and to develop applications, the selective control of the spatial position of an individual CN and the selective sorting of CNs are strongly desired by lots of researchers and industrial engineers. Utilizing the resonant radiation force mediated by excitons is one of the promising techniques for this purpose. The radiation force reflects the size quantization of exciton levels and changes significantly depending on the geometric properties such as the size and shape of the target nano-object. As theoretically proposed,[15–17] this enables us to selectively manipulate specific nano-objects. Recently, it has been experimentally demonstrated that, by using resonant radiation force, the transport of semiconductor nanoparticles with diameters of several tens of nanometers over macroscopic distance is possible.[18] This experiment has been performed in superfluid helium in order to utilize the maximum performance of the resonant radiation force. Further, there are several experimental reports demonstrating the resonant enhancement of the radiation force exerted on organic nanoparticles.[19,20]

In the case of SWCNs, it has been reported that slight enrichment of semiconducting SWCNs was observed by using an optical trap.[21] Recently, SWCNs with similar diameters have been aggregated by using a strongly focused laser beam,[22] where several kinds of structures have been determined by using resonant Raman spectra of the radial breathing modes. The analysis in this experiment has been limited to the joint density of states calculated by using a tight-binding model without considering the exciton effect. However, the excitonic resonance strongly characterizes the resonant optical manipulation and thus, it is essential to consider this effect to reveal the characteristics of phenomena. At almost the same time as the publication of Ref. 22, we briefly reported a theoretical investigation of the radiation force mediated by exciton of SWCNs for propagating laser field.[23] In our previous work, exciton states around K and K' points were treated independently. However, optically allowed or bright states of exciton form bonding states of singlet K and K' excitons.[24] Therefore, in this paper, we calculate the radiation force mediated by the bright exciton states in great detail. As a conclusion, the strength of radiation force is found to be not modified. Here, we shall also calculate gradient force on SWCNs for optical trapping. We use our developed theoretical framework,[17,25] which is based on the microscopic optical-response theory.[26]

Optical-absorption spectra of a SWCN have been calculated without considering Coulomb interactions; the spectra reflect the dependence of the electronic states on the size, manner of rolled up, and applied magnetic field.[27,28] A promi-

nent excitonic effect of a SWCN has been predicted in the form of a large binding-energy and steep absorption peaks due to its quasi-one-dimensionality.[29] This prediction has been confirmed by absorption[30,31] and luminescence spectra[32–35] at room temperature. Owing to the steepness of the absorption peaks and strong size dependence of the peak position, size-selective manipulation of SWCNs is possible. Furthermore, optical spectra of SWCNs exhibit strong polarization dependence; a spectral peak is suppressed,[27,36] and the peak position moves toward a higher energy[36] for perpendicular polarization because of the depolarization effect. This strong anisotropy would be useful for the manipulation and sorting of SWCNs whose major axial orientation is parallel to the direction of light polarization.

This paper is organized as follows: In Sec. II, exciton states are briefly summarized. The calculation method for the optical response is given in Sec. III. In this formulation, the electromagnetic (EM) field and induced current density due to excitons are determined self-consistently. Then, the self-energy of the exciton via EM field is included in the resulting optical response. We evaluate the magnitude of the self-energy in this section. In Sec. IV, the dissipative radiation force for the traveling EM field and potential due to the gradient force for the standing EM field are studied. In Sec. V, the potential due to the gradient force is calculated taking the band warping effect into consideration in order to study the possibility of fine selective manipulation of SWCNs with a specific structure. The summary and conclusion are given in Sec. VI.

II. EXCITON STATES

An SWCN has the structure of a rolled-up two-dimensional (2D) graphite sheet, in which the conduction and valence π bands touch at K and K' points. When the diameter is sufficiently large, the effect of the π and σ bands mixing can be neglected. Then, the electronic states of the SWCN are obtained by imposing a boundary condition in the circumference direction on the electronic states of the graphite sheet. We choose the x and y coordinates in the circumference and axial directions, respectively [see Figs. 1(a) and 1(b)]. The $\mathbf{k}\cdot\mathbf{p}$ equation around the K point of the graphite sheet is given by

$$\gamma[\sigma_x\hat{k}_x + \sigma_y\hat{k}_y]\mathbf{F}^K(\mathbf{r}) = \varepsilon\mathbf{F}^K(\mathbf{r}), \tag{1}$$

where γ is a band parameter, σ_x and σ_y are the Pauli spin matrices, $\hat{\mathbf{k}} \equiv -i\boldsymbol{\nabla}$ is the wave-vector operator, and ε is the eigenenergy. $\mathbf{F}^K(\mathbf{r})$ is the envelope function with two components representing the amplitude at two carbon atoms in a unit cell. The two atomic sites are indicated by A and B in Fig. 1(a). The Fermi level lies at $\varepsilon=0$ when the material is undoped. The boundary condition for $\mathbf{F}^K(\mathbf{r})$ is given by

$$\mathbf{F}^K(\mathbf{r}+\mathbf{L}) = \mathbf{F}^K(\mathbf{r})\exp\left[2\pi i\left(\varphi - \frac{\nu}{3}\right)\right], \tag{2}$$

where we generalize the boundary condition in the presence of an AB magnetic flux $\varphi=\phi/\phi_0$, with magnetic-flux quantum $\phi_0=ch/e$.[6] The integer ν is 0, +1, or −1, from the relation $n_a+n_b=3M+\nu$ with integer M; here, $\mathbf{L}=n_a\mathbf{a}+n_b\mathbf{b}$ is the chiral vector with $\mathbf{a}$ and $\mathbf{b}$ being the primitive translation vectors of the 2D graphite shown in Fig. 1(a). The structure of each SWCN can be uniquely determined by the chiral vector in the circumference direction. The resulting energy of a SWCN is given by

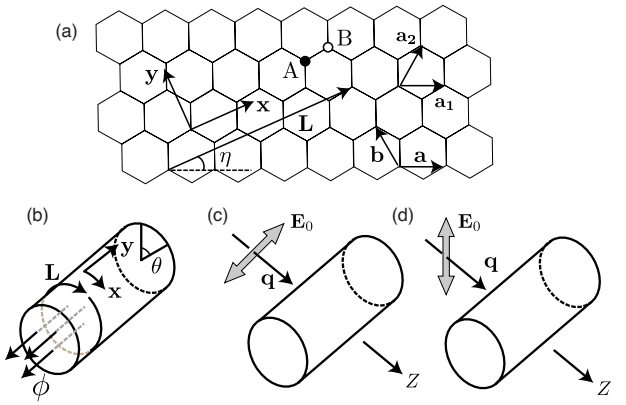

FIG. 1. (Color online) (a) The lattice structure of 2D graphite and the coordinate system. Two primitive translation vectors are denoted by **a** and **b**, a chiral vector of a SWCN is denoted by **L**, x and y are set in the circumference and axial directions, respectively, η denotes a chiral angle, and A and B represent two types of carbon sites. Other choice for the primitive translation vectors are denoted by $\mathbf{a}_1$ and $\mathbf{a}_2$. (b) The coordinate system (x,y) and θ. An AB flux ϕ is also depicted. (c) Schematic illustration of an applied EM field with polarization parallel to the tube axis. (d) Illustration of an applied EM field with perpendicular polarization. The direction of the wave vector **q** of the EM field is indicated by "Z" perpendicular to the tube axis.

$$\varepsilon^K_{\pm n}(k) = \pm\gamma\sqrt{\kappa_{\nu\varphi}(n)^2 + k^2} \tag{3}$$

with

$$\kappa_{\nu\varphi}(n) = \frac{2\pi}{L}\left(n - \frac{\nu}{3}\right), \tag{4}$$

where + and − correspond to conduction and valence states, respectively. Around the K' point, the $\mathbf{k}\cdot\mathbf{p}$ equation and the boundary condition are obtained by replacing σ_y with $-\sigma_y$ and ν with $-\nu$. In this approximation, the electronic states of a SWCN depend only on its diameter; the SWCN is metallic for $\nu=0$ and is semiconducting with energy gap $4\pi\gamma/3L$ for $\nu=\pm1$. An AB flux changes the band gap ranging from 0 to $2\pi\gamma/L$ in the period of ϕ_0.[6]

An excited conduction electron and a valence hole form an exciton state mainly due to the long-range Coulomb interaction between them. Since there are two valleys at the K and K' points and twofold spin degeneracy exists, the exciton states have 16-fold degeneracy.[24] For example, we have singlet exciton states with both electron and hole in the K valley

$$^1|KK\rangle = \frac{1}{\sqrt{2}}[|(K,\uparrow)(K,\uparrow)\rangle + |(K,\downarrow)(K,\downarrow)\rangle], \quad (5)$$

where $|(\upsilon,\sigma)(\upsilon',\sigma')\rangle$ with υ, $\upsilon'=K$, or K' and σ, $\sigma'=\uparrow$, or $\downarrow$ denotes the exciton state for an electron with spin σ in valley υ and hole with spin σ' in valley υ'. Among the degenerate levels, we focus on an optically allowed level[24] given by

$$^1|KK-K'K'(+)\rangle = \frac{1}{\sqrt{2}}(^1|KK\rangle + ^1|K'K'\rangle). \quad (6)$$

Exciton states $|(\upsilon,\sigma)(\upsilon,\sigma)\rangle$ are further specified by the wave vector $2\pi l/L$ around the tube axis and the level index u, and thus, they can be expanded as

$$|(\upsilon,\sigma)(\upsilon,\sigma)\rangle_{u,l} = \sum_{n,k} \psi^{\upsilon}_{u,l}(n,k) c^{\upsilon,\dagger}_{+,n+l,k,\sigma} c^{\upsilon}_{-,n,k,\sigma}|g\rangle, \quad (7)$$

where $c^{\upsilon}_{\pm,n,k,\sigma}$ is the annihilation operator for an electron with spin σ near the $\upsilon=K$ or K' point with energy $\varepsilon^{\upsilon}_{\pm n}(k)$. It is noted that the exciton wave function $\psi^{\upsilon}_{u,l}(n,k)$ is independent of spin states and thus, $^1|\upsilon\upsilon\rangle_{u,l}=\sqrt{2}|(\upsilon,\uparrow)(\upsilon,\uparrow)\rangle_{u,l}$ $=\sqrt{2}|(\upsilon,\downarrow)(\upsilon,\downarrow)\rangle_{u,l}\equiv\sqrt{2}|\upsilon\upsilon\rangle_{u,l}$. We denote the optically allowed states $^1|KK-K'K'(+)\rangle$ by $|u,l\rangle$; then,

$$|u,l\rangle = |KK\rangle_{u,l} + |K'K'\rangle_{u,l}. \quad (8)$$

In order to obtain the wave function $\psi^{\upsilon}_{u,l}(n,k)$, we use the screened Hartree-Fock approximation in terms of the effective-mass or $\mathbf{k}\cdot\mathbf{p}$ approximation.[29]

The band parameter γ is related to the hopping integral γ_0 as $\gamma=(\sqrt{3}/2)a\gamma_0$ with lattice constant $a=2.46$ Å in a nearest-neighbor tight-binding model. It should be noted that the experimentally determined γ is renormalized by electron-electron interaction. This renormalized part should be excluded in the screened Hartree-Fock approximation; otherwise, the electron-electron interaction is overcounted. It has been shown that $\gamma_0\approx 2.7$ eV reproduces the observed one- and two-photon absorption energies in semiconducting SWCNs in the screened Hartree-Fock approximation.[37] The strength of the Coulomb interaction is characterized by $\tilde{v}=(e^2/\kappa_c L)/(2\pi\gamma/L)$ independent of L, where κ_c is the effective static dielectric constant of the SWCN. The Coulomb interaction $\tilde{v}$ which lies between 0.1 and 0.2, describes the experimental results well.[37,38] We set $\tilde{v}=0.15$ in the following calculation.

The $\mathbf{k}\cdot\mathbf{p}$ scheme is applicable near the Fermi energy and thus, a cutoff function given by $g_0(\varepsilon)=\varepsilon_c^{\alpha_c}/(|\varepsilon|^{\alpha_c}+\varepsilon_c^{\alpha_c})$ is introduced when summations for the band index and wave vector are necessary. The parameters ε_c and α_c should be chosen in such a way that only the contribution from states near the Fermi energy is included. However, a finite result is obtained for infinite ε_c in some cases: magnetic properties,[39] spontaneous in-plane Kekule, and out-of-plane lattice distortions,[40] acoustic-phonon distributions,[41] etc. In the calculation of exciton states, the band-gap shift shows weak logarithmic dependence on the cutoff energy.[38] In such cases, the cutoff ε_c should be chosen as the π bandwidth of the 2D graphite. For a typical SWCN with $d\approx 1.4$ nm, the cutoff energy is about $\varepsilon_c/(2\pi\gamma/L)\approx 10$, which is used in the following calculations. For a fixed cutoff parameter ε_c, the exciton states are universally expressed independent of the circumference L if the length is scaled by L and the energy is scaled by $2\pi\gamma/L$ in the $\mathbf{k}\cdot\mathbf{p}$ scheme.

III. SELF-CONSISTENT TREATMENT

When an EM field is applied to a SWCN, a current density due to the exciton is induced. The induced current density generates an EM field, which in turn induces a current density. Therefore, the EM field and induced current density are determined self-consistently. We calculate the self-consistent fields by using a microscopic optical-response theory.[26,42,43] The resulting fields include radiative correction: radiative decay width and radiative shift of the resonant-excitation frequency. A depolarization field, which appears for EM fields polarized perpendicular to the tube axis, is also included in the self-consistent field. This microscopic optical-response theory provides a unified treatment of the radiative correction and depolarization effect, which are described by the self-energy of exciton in EM fields. In addition, the scattering force related to the radiative decay width can be calculated in this treatment. As shown later, the dissipative forces exerted by propagating waves are classified as scattering and absorption forces. The absorption force is related to the nonradiative decay width. The present formula provides the respective contributions of the scattering and absorption forces in the dissipative force. This is useful for discussing the temperature dependence of the dissipative force in terms of the nonradiative decay width.

The generated EM field is calculated by convoluting the Green's function for the Maxwell equations with the current density. In the original version of the microscopic optical-response theory, the transverse component of the Green's function should be extracted. Here, we use a revised version, where the full Green's function can be used without splitting it into the transverse and longitudinal components.[43] The current density due to the exciton is given by

$$\mathbf{j}(\mathbf{r},\omega) = \int d\mathbf{r}'\overline{\boldsymbol{\sigma}}(\mathbf{r},\mathbf{r}')\cdot\mathbf{E}(\mathbf{r}',\omega) \quad (9)$$

with $\overline{\boldsymbol{\sigma}}$ being a conductivity tensor,

$$\overline{\boldsymbol{\sigma}}(\mathbf{r},\mathbf{r}') = \frac{\hbar}{i}\sum_{u,l}\frac{1}{E_{u,l}}\frac{\langle g|\hat{\mathbf{j}}(\mathbf{r})|u,l\rangle\langle u,l|\hat{\mathbf{j}}(\mathbf{r}')|g\rangle}{E_{u,l}-\hbar\omega-i\hbar\Gamma}, \quad (10)$$

where $\mathbf{E}$ is the total EM field consisting of the applied field $\mathbf{E}_0$ and the scattered field, $E_{u,l}$ is the energy of the exciton state $|u,l\rangle$, $|g\rangle$ is the ground state, and Γ is a phenomenological nonradiative damping constant. The current-density operator $\hat{\mathbf{j}}(\mathbf{r})$ at the K point is given by

$$\hat{j}_\xi(\mathbf{r}) = -\frac{e\gamma}{\hbar}\sigma_\xi\delta(\hat{\mathbf{r}}-\mathbf{r}) \quad (\xi=x,y). \quad (11)$$

The operator $\hat{j}_x(\mathbf{r})$ at the K' point is the same as that at the K point while $\hat{j}_y(\mathbf{r})$ at the K' point has the opposite sign of that at the K point. The induced current density produces the scattered field. Then, the total EM field is written as

$$\mathbf{E}(\mathbf{r}) = \mathbf{E}_0(\mathbf{r}) + \int d\mathbf{r}' \overline{\mathbf{G}}(\mathbf{r},\mathbf{r}') \cdot \mathbf{j}(\mathbf{r}'), \tag{12}$$

where $\overline{\mathbf{G}}$ is a dyadic Green's function for the Maxwell equations satisfying

$$\boldsymbol{\nabla} \times \boldsymbol{\nabla} \times \overline{\mathbf{G}}(\mathbf{r},\mathbf{r}') - \kappa_{\mathrm{bg}}(\mathbf{r}) q_0^2 \overline{\mathbf{G}}(\mathbf{r},\mathbf{r}') = \mathbf{I}\delta(\mathbf{r}-\mathbf{r}'), \tag{13}$$

where κ_{bg} is the background dielectric constant, $q_0 = \omega/c$, and $\mathbf{I}$ is the identity tensor. The Green's functions can be analytically expressed for simple inhomogeneous media such as single-layer or multilayer structures of slabs, cylinders, and spheres.[44] In the effective-mass approximation, the envelope function $\mathbf{F}^K(\mathbf{r})$ smoothly varies beyond lattice structure of carbon atoms. Therefore, the dyadic Green's function without taking account of lattice structure is safely applicable under the effective-mass approximation. The dyadic Green's function for a hollow cylindrical shape with a surrounding background dielectric constant κ_{bg} is given by

$$G_{yy}(\mathbf{r},\mathbf{r}') = -\frac{q_0^2}{2\omega\kappa_{\mathrm{bg}}} \sum_{n=-\infty}^{\infty} \int_{-\infty}^{\infty} dk_y (-1)^n \times J_n(qa) H_n^{(1)}(qa) e^{ik_y(y-y')} e^{in(\theta-\theta')},$$

$$G_{xx}(\mathbf{r},\mathbf{r}') = -\frac{q_0^2}{8\omega\kappa_{\mathrm{bg}}} \sum_{n=-\infty}^{\infty} \int_{-\infty}^{\infty} dk_y (-1)^{n+1} \times [J_{n-1}(qa) - J_{n+1}(qa)][H_{n-1}^{(1)}(qa) - H_{n+1}^{(1)}(qa)] \times e^{ik_y(y-y')} e^{in(\theta-\theta')}, \tag{14}$$

where $q = \sqrt{\kappa_{\mathrm{bg}}} q_0$, θ is the azimuth depicted in Fig. 1(b), and $J_n(qa)$ and $H_n^{(1)}(qa)$ are the Bessel function and Hankel function of the first kind, respectively. Substituting Eq. (9) into Eq. (12), we have

$$\mathbf{E}(\mathbf{r}) = \mathbf{E}_0(\mathbf{r}) + \frac{\hbar}{i} \sum_{u,l} \int d\mathbf{r}' \overline{\mathbf{G}}(\mathbf{r},\mathbf{r}') \cdot \frac{\langle g|\hat{\mathbf{j}}(\mathbf{r}')|u,l\rangle}{E_{u,l}} X_{u,l}, \tag{15}$$

with

$$X_{u,l} = \frac{1}{E_{u,l} - \hbar\omega - i\hbar\Gamma} \int d\mathbf{r} \langle u,l|\hat{\mathbf{j}}(\mathbf{r})|g\rangle \cdot \mathbf{E}(\mathbf{r}). \tag{16}$$

By multiplying $\langle u,l|\hat{\mathbf{j}}(\mathbf{r})|g\rangle$ with the left-hand side of Eq. (15) and integrating with respect to $\mathbf{r}$, the self-consistent equations for $X_{u,l}$ are derived as follows:

$$\sum_{u'} [(E_{u,l} - \hbar\omega - i\hbar\Gamma)\delta_{uu'} + A_{uu',l}] X_{u',l} = B_{u,l}^{(0)} \tag{17}$$

with

$$A_{uu',l} = \frac{i\hbar}{E_{u',l}} \int d\mathbf{r} \int d\mathbf{r}' \langle u,l|\hat{\mathbf{j}}(\mathbf{r})|g\rangle \cdot \overline{\mathbf{G}}(\mathbf{r},\mathbf{r}') \cdot \langle g|\hat{\mathbf{j}}(\mathbf{r}')|u',l\rangle, \tag{18}$$

$$B_{u,l}^{(0)} = \int d\mathbf{r} \langle u,l|\hat{\mathbf{j}}(\mathbf{r})|g\rangle \cdot \mathbf{E}_0(\mathbf{r}). \tag{19}$$

The factor $A_{uu',l}$ represents a self-interaction of induced current density via EM field. It is noted that the dyadic Green's function includes both transverse and longitudinal components. The interaction via transverse EM field provides radiative correction while the interaction via longitudinal component provides the depolarization shift of spectral peaks toward the higher energies. This longitudinal component can be considered to be a long-range electron-hole exchange interaction.[43] Since the depolarization effect in Ref. 36 is calculated by using the background dielectric of graphite, we use $\kappa_c = 2.4$ for graphite in the evaluation of $A_{uu',l}$. For the other evaluation, the background dielectric is set to $\kappa = 1$ as the surroundings of SWCNs to be vacuum.

The exciton self-energy via EM field $\tilde{E}_{u,l}$ is obtained as the energy of a self-sustaining mode without the applied field $\mathbf{E}_0$, i.e., $B_{u,l}^{(0)} = 0$. Then, from Eq. (17) without the damping constant Γ, we obtain equations for $\tilde{E}_{u,l}$ as follows:

$$\sum_{u'} (E_{u,l}\delta_{uu'} + A_{uu',l}) X_{u',l} = \hbar\omega X_{u,l}, \tag{20}$$

where solutions for $\hbar\omega$ correspond to $\tilde{E}_{u,l}$. These simultaneous equations are nonlinear because ω or q is included as an argument of Bessel functions in the dyadic Green's function through $A_{uu',l}$. We can iteratively solve the nonlinear simultaneous equations. The self-energy of the exciton via EM field is given by $\Delta E_{u,l} \equiv \tilde{E}_{u,l} - E_{u,l}$.

Let us introduce an "individual-exciton approximation," where the self-interaction between different exciton states is neglected. Then, the self-interaction represented by a matrix can be approximated by the scalar of the diagonal matrix element, i.e., $A_{uu',l} = \delta_{uu'} A_{uu,l}$, and the exciton energy including the self-interaction $\tilde{E}_{u,l}$ is given by

$$\tilde{E}_{u,l} = \bar{E}_{u,l} + i\Gamma_{u,l}^{\mathrm{rad}}, \tag{21}$$

where $\bar{E}_{u,l} \equiv E_{u,l} + \mathrm{Re}(A_{uu,l})$ is a resonant-excitation energy including the radiative shift $\mathrm{Re}(A_{uu,l})$ and $\Gamma_{u,l}^{\mathrm{rad}} \equiv -\mathrm{Im}(A_{uu,l})$ is a radiative decay line width. These physical meanings of $\bar{E}_{ul}$ and $\Gamma_{u,l}^{\mathrm{rad}}$ are clearly represented in Eq. (34). The self-energy of the exciton is given by $\Delta E_{u,l} = A_{uu,l}$. This approximation is valid when the self-interaction is much smaller than the separation of exciton energies.

A. Parallel polarization

When the polarization of an applied EM field is parallel to the tube axis, as shown in Fig. 1(c), the strength of the electric field is almost independent of the circumference position because the wavelength of the EM field is much longer than the diameter of the SWCN. Therefore, the exciton states with $l = 0$ are excited due to the wave-vector conservation in the circumference direction.

In the individual-exciton approximation, the self-energy of the exciton, $\Delta E_{\parallel} \equiv \Delta E_{u,0} = A_{uu,0}$, for parallel polarization is given by

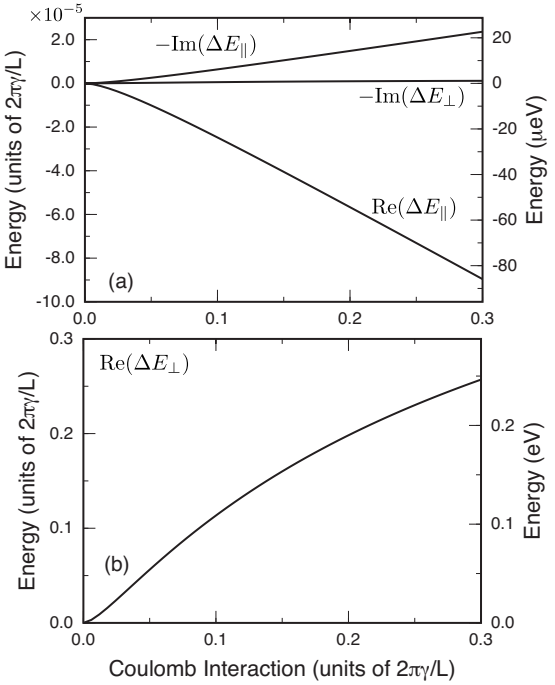

FIG. 2. Self-energy of an exciton via EM field as a function of Coulomb interaction. The energy on the vertical axis to the right is calculated for a SWCN with $d=1.2$ nm. (a) Real $[\mathrm{Re}(\Delta E_{\|})]$ and imaginary $[-\mathrm{Im}(\Delta E_{\|})]$ parts of the self-energy of the lowest exciton for parallel polarization and the imaginary part $[-\mathrm{Im}(\Delta E_{\perp})]$ of the self-energy of the lowest exciton for perpendicular polarization. (b) Real part $[\mathrm{Re}(\Delta E_{\perp})]$ of the self-energy of the lowest exciton for perpendicular polarization.

$$\Delta E_{\|} = \frac{2\pi\gamma}{L}\pi\left(\frac{\gamma}{\hbar c}\right)^2 \frac{\hbar\omega}{E_{u,0}}\tilde{v}|\tilde{j}_y^{u,0}|^2\left[\frac{2}{\pi}\left(\gamma' + \log\frac{qL}{4\pi}\right) - i\right], \tag{22}$$

where $\gamma'=0.57722$ is Euler's constant, $\tilde{v}=(e^2/\kappa_c L)/(2\pi\gamma/L)$ ranges from approximately 0.1 to 0.2,[37,38] and $\tilde{\mathbf{j}}^{u,0}$ has a dimensionless value of order 1 defined by $\langle u,0|\mathbf{j}(\mathbf{r})|g\rangle=(e\gamma/\hbar)(L^3A)^{-1/2}\tilde{\mathbf{j}}^{u,0}$. Therefore, the orders of both $\mathrm{Re}[\Delta E_{\|}]$ and $\mathrm{Im}[\Delta E_{\|}]$ are determined by $[\gamma/(\hbar c)]^2 \approx 10^{-5}$ for $\gamma_0=2.7$ eV in units of $2\pi\gamma/L$, where $(\gamma/\hbar)/c$ represents the ratio of the Fermi velocity of an electron in a SWCN to the light velocity.

Figure 2(a) shows the $\mathrm{Re}(\Delta E_{\|})$ and $-\mathrm{Im}(\Delta E_{\|})$ of the lowest exciton state as a function of the Coulomb interaction $\tilde{v}$. These real and imaginary parts of the self-energy are obtained by solving the simultaneous nonlinear equation (20). The energy on the vertical axis to the right is evaluated for a SWCN with a diameter $d=1.2$ nm. The intrinsic radiative decay width $[\hbar\Gamma_{u,0}^{\mathrm{rad}}=-\mathrm{Im}(\Delta E_{\|})]$ is ≈ 10 μeV for $\tilde{v}=0.15$. This radiative width corresponds to an intrinsic radiative lifetime of ≈ 65 ps.

It has been reported that the intrinsic radiative lifetime of a zigzag SWCN with $d=0.78$ nm is 19.1 ps in the *ab initio* calculation.[45] The radiative lifetime is proportional to the diameter and thus, the extrapolated lifetime in the *ab initio* calculation becomes 84 ps for a SWCN with $d=1.2$ nm. The radiative lifetime in the present calculation is similar to that in the *ab initio* calculation. The effective radiative lifetime is longer than the intrinsic radiative lifetime because of the thermal distribution of exciton states and the existence of a dark exciton. The enhancement factor of the effective radiative lifetime due to the thermalization is proportional to the square root of temperature for a quantum wire[46] and this factor for a SWCN at room temperature is ≈ 100.[45] The effect of a dark exciton on the effective lifetime depends on the level splitting of bright and dark states.[45] In a recent experiment performed for individual SWCNs, the observed level splitting was approximately about 4 meV.[8] This level splitting enhances the effective radiative lifetime by a factor of 2.2. Consequently, in our calculation, the effective radiative lifetime is 14 ns. This value is in rough agreement with the experimental result of ~ 10 ns.[47]

B. Perpendicular polarization

When the polarization of the applied EM field is perpendicular to the tube axis, as shown in Fig. 1(d), the strength of the electric field changes sinusoidally in the circumference direction. Therefore, exciton states with $l=\pm 1$ can be excited. In the individual-exciton approximation, the self-energy $\Delta E_{\perp} \equiv A_{uu,\pm 1}$ is given by

$$\Delta E_{\perp} = \frac{2\pi\gamma}{L}\frac{\pi}{4}\left(\frac{\gamma}{\hbar c}\right)^2 \frac{\hbar\omega}{E_{u,\pm 1}}\tilde{v}|\tilde{j}_x^{u,\pm 1}|^2\left[\frac{16\pi}{(qL)^2} - i\right]. \tag{23}$$

The order of $\mathrm{Im}(\Delta E_{\perp})$ is 10^{-5} in units of $2\pi\gamma/L$ as well as the self-energy of exciton for parallel polarization. In Fig. 2(a), $-\mathrm{Im}(\Delta E_{\perp})$ for the lowest exciton state is shown as a function of Coulomb interaction $\tilde{v}$. The radiative decay width for $\tilde{v}=0.15$ is about one tenth of that for parallel polarization.

In contrast to other real and imaginary parts of the self-energy $[\mathrm{Re}(\Delta E_{\|}), -\mathrm{Im}(\Delta E_{\|}), -\mathrm{Im}(\Delta E_{\perp})]$, $\mathrm{Re}(\Delta E_{\perp})$ exhibits quite a different order of magnitude, as shown in Fig. 2(b). This is because $\mathrm{Re}(\Delta E_{\perp})$ contains a factor $16\pi/(qL)^2 = (4/\pi^3)(\lambda/d)^2 \approx 10^4$, with d being the diameter of the SWCN. In conjunction with $[\gamma/(\hbar c)]^2 \approx 10^{-5}$, we have $\mathcal{O}[\mathrm{Re}(\Delta E_{\perp})] \approx 0.1$. $\mathrm{Re}(\Delta E_{\perp})$ takes a finite value under the condition $c \to \infty$, and thus, this term represents the static Coulomb interaction between induced current density of exciton. This effect has been included in the calculation of the absorption spectra of SWCNs by taking into account the depolarization field.[36] When a polarized field perpendicular to the tube axis is applied, a spatially inhomogeneous current is induced in the circumference direction. This inhomogeneous current produces a charge distribution, which generates the depolarization field. The depolarization effect is accounted for in the dielectric function $\varepsilon_{xx}^{\pm 1}(\omega)$. Then, the excitation energy is given by the zero points ω_0 of $\varepsilon_{xx}^{\pm 1}(\omega)$,

$$\varepsilon_{xx}^{\pm 1}(\omega_0) = 1 + A\frac{8\pi^2\hbar}{\kappa\omega_0}\sum_{KK'}\sum_{u}\frac{|\langle u,\pm 1|\hat{j}_x|g\rangle|^2}{E_{u,\pm 1}(E_{u,\pm 1}-\hbar\omega_0)} = 0, \tag{24}$$

where A is the length of the SWCN. This equation is derived from Eq. (46) in Ref. 36 by using the rotating wave approxi-

mation, eliminating the nonradiative damping constant, and replacing the matrix element of the current operator by that in our definition. In the individual-exciton approximation, this equation can be recast as

$$\hbar\omega_0 = E_{u,\pm 1} + 2\sum_{\zeta=KK'} \mathrm{Re}[A^{\zeta}_{uu,\pm 1}(\omega_0)], \tag{25}$$

where $A^{K}_{uu,\pm 1}$ ($A^{K'}_{uu,\pm 1}$) is the self-interaction for the exciton state $|KK\rangle_{u,l}$ ($|K'K'\rangle_{u,l}$) but the bright states $|u,l\rangle$. In the absence of magnetic flux ϕ, $|KK\rangle$ and $|K'K'\rangle$ provide the same contribution to the induced current density, i.e., $\langle g|\hat{\mathbf{j}}(\mathbf{r})|KK\rangle = \langle g|\hat{\mathbf{j}}(\mathbf{r})|K'K'\rangle = (1/2)\langle g|\hat{\mathbf{j}}(\mathbf{r})|u,l\rangle$. The self-interaction is proportional to the square of the induced current density and thus, $A^{K}_{uu,\pm 1} = A^{K'}_{uu,\pm 1} = (1/4)A_{uu,\pm 1}$. Substituting this quantity into Eq. (25), we have $\hbar\omega_0 = E_{u,\pm 1} + \mathrm{Re}[A_{uu,\pm 1}(\omega_0)] = \bar{E}_{u,\pm 1}$. Therefore, the analytic expression of excitation energy including the depolarization shift in Ref. 36 agrees with the expression in our self-consistent treatment if we use the individual-exciton approximation.

IV. RADIATION FORCE

The self-consistently determined current density is written in terms of $X_{u,l}$ as follows:

$$\mathbf{j}(\mathbf{r}) = \frac{\hbar}{i}\sum_{u,l} \frac{\langle g|\hat{\mathbf{j}}(\mathbf{r})|u,l\rangle}{E_{u,l}} X_{u,l}. \tag{26}$$

Substituting this into Eq. (12), we have the following EM field:

$$\mathbf{E}(\mathbf{r}) = \mathbf{E}_0(\mathbf{r}) + \frac{\hbar}{i}\sum_{u,l}\int d\mathbf{r}'\overline{\mathbf{G}}(\mathbf{r},\mathbf{r}')\cdot\frac{\langle g|\hat{\mathbf{j}}(\mathbf{r}')|u,l\rangle}{E_{u,l}} X_{u,l}. \tag{27}$$

A radiation force $\mathbf{F}$ exerted on a SWCN is calculated from a general expression[17,25]

$$\mathbf{F}(\omega) = \frac{1}{2}\mathrm{Re}\left\{\frac{i}{\omega}\int d\mathbf{r}[\nabla\mathbf{E}^*(\mathbf{r},\omega)]\cdot\mathbf{j}(\mathbf{r},\omega)\right\}. \tag{28}$$

In the following calculations, $\mathbf{E}(\mathbf{r})$ in Eq. (28) can be replaced by $\mathbf{E}_0(\mathbf{r})$ because the contribution from the scattered field is cancelled out due to the symmetry. This expression includes both dissipative (absorption and scattering) and gradient forces. When a propagating EM field is applied to an object, the dissipative force is exerted in the applied field direction due to the momentum transfer from a photon to the object. When the EM field intensity has spatial inhomogeneity, a gradient force is exerted on the SWCN. By using the gradient force, microscopic dielectric objects can be physically held and moved; this scientific instrument is called optical tweezers.[48]

A. Dissipative force

First, we consider a situation in which a propagating plane EM field is applied to a SWCN. The EM field has a wave vector $\mathbf{q}$ perpendicular to the tube axis, whose direction is denoted by Z [see Figs. 1(c) and 1(d)]. Then, the applied EM field is written as $\mathbf{E}_0 = E_0\mathbf{e}_{\parallel,\perp}e^{iqZ}$, where $\mathbf{e}_{\parallel}$ and $\mathbf{e}_{\perp}$ represent unit polarization vectors parallel and perpendicular to the tube axis, respectively. Consequently, the dissipative force $\mathbf{F}$ is exerted in the Z direction and the force is expressed as

$$F_Z(\omega) = \frac{\sqrt{\kappa}}{c}P(\omega) + \frac{\hbar}{2}\frac{\sqrt{\kappa}}{c}\sum_{uu'l}\frac{\mathrm{Im}(X_{u,l}A^*_{uu',l}X^*_{u',l})}{E_{u,l}} \tag{29}$$

with

$$P(\omega) = \frac{1}{2}\int d\mathbf{r}\ \mathrm{Re}[\mathbf{j}^*(\mathbf{r})\cdot\mathbf{E}(\mathbf{r})] = \frac{\hbar^2\Gamma}{2}\sum_{u,l}\frac{|X_{u,l}|^2}{E_{u,l}} \tag{30}$$

being the optical absorption. The first and second terms on the right-hand side of Eq. (29) represent absorption and scattering forces, respectively. The scattering force becomes zero if we neglect the self-interaction.

In order to study the characteristics of the dissipative force, we represent the expression of Eq. (29) by the individual-exciton approximation. Furthermore, the frequency dependence of $A_{uu,l}$ is neglected by setting $\hbar\omega = E_{u,l}$. This approximation gives the spectral shape and indicates a clear dependence of the nonradiative decay width on the dissipative force. We consider that a parallel-polarized EM field is applied, i.e., exciton with $l=0$ is excited. From $J_0(qa \approx 0) \approx 1$, $B^{(0)}_{u,0}$ is approximated as

$$B^{(0)}_{u,0} \approx \frac{e\gamma}{\hbar}\sqrt{\frac{A}{L}}\tilde{j}^{u,0}_y E_0. \tag{31}$$

Then, the relationship between the radiative decay width $\hbar\Gamma^{\mathrm{rad}}_{u,0} = -\mathrm{Im}[A_{uu,0}]$ and $B^{(0)}_{u,0}$ is obtained as follows:

$$|B^{(0)}_{u,0}|^2 = \kappa_c c^2\frac{AE_0^2}{\pi}\Gamma^{\mathrm{rad}}_{u,0}. \tag{32}$$

In the individual-exciton approximation, $X_{u,0}$ determined from Eq. (17) is given by

$$X_{u,0} = \frac{B^{(0)}_{u,0}}{\bar{E}_{u,0} - \hbar\omega - i\hbar(\Gamma + \Gamma^{\mathrm{rad}}_{u,0})}. \tag{33}$$

Finally, the dissipative force $F^{\parallel}_Z$ for parallel polarization is approximated as

$$F^{\parallel}_Z(\omega) = 4\kappa_c A I_0 \sum_u \frac{\hbar\Gamma^{\mathrm{rad}}_{u,0}}{E_{u,0}}\frac{\hbar\Gamma + \hbar\Gamma^{\mathrm{rad}}_{u,0}}{(\bar{E}_{u,0} - \hbar\omega)^2 + (\hbar\Gamma + \hbar\Gamma^{\mathrm{rad}}_{u,0})^2}, \tag{34}$$

where $I_0 \equiv \sqrt{\kappa}cE_0^2/(8\pi)$ is the applied field intensity. The dissipative force spectra have a Lorentzian line shape. As described in relation to Eq. (21), $\bar{E}_{u,0}$ and $\Gamma^{\mathrm{rad}}_{u,0}$ represent the resonant-excitation energy and decay line width, respectively. The first and second terms in the numerator correspond to the absorption and scattering forces, respectively. It is noted that the nonradiative decay width is a few meV even at low temperatures (a few K) while the radiative decay width is 20 μeV at most [see Fig. 2(a)]. Therefore, the ab-

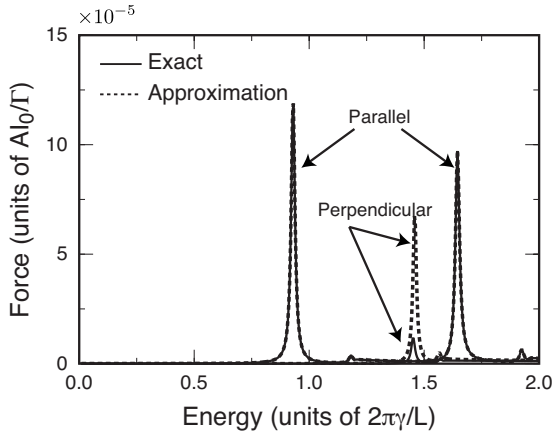

FIG. 3. Calculated dissipative force exerted on a SWCN for parallel and perpendicular polarizations (solid lines). Coulomb interaction is set to be $\tilde{v}=0.15$. The dotted lines denote the results calculated by using the individual-exciton approximation.

sorption force proportional to Γ in Eq. (34) dominates the dissipative force.

At the resonant-excitation condition, $\bar{E}_{u,0}-\hbar\omega=0$ in Eq. (34), the dissipative force is given by

$$F_Z^{\parallel,\mathrm{res}} \approx 4\kappa_c A I_0 \frac{1}{E_{u,0}} \frac{\Gamma_{u,0}^{\mathrm{rad}}}{\Gamma+\Gamma_{u,0}^{\mathrm{rad}}}. \tag{35}$$

Since Γ is much larger than $\Gamma_{u,0}^{\mathrm{rad}}$ even at low temperatures of a few K, the resonant dissipative force is proportional to $1/\Gamma$. The resonant dissipative force monotonically increases with decreasing Γ and eventually reaches a maximum $F_Z^{\parallel,\mathrm{res}}=4\kappa_c A I_0/E_{u,0}$ at $\Gamma=0$. The maximum dissipative force at the resonant condition is independent of the current density or oscillator strength. However, the line width $\Gamma_{u,0}^{\mathrm{rad}}$ of the radiation force is proportional to the oscillator strength, and thus, the integrated force is proportional to the oscillator strength.

Figure 3 shows the calculated dissipative force for parallel and perpendicular polarizations. The force is proportional to the length of SWCNs and the intensity of the applied field. The resonant radiation force is proportional to $1/\Gamma$, except for extremely low temperatures, and thus, we choose AI_0/Γ as the unit of force. The results obtained by using the individual-exciton approximation are denoted by dotted lines. The individual-exciton approximation describes the radiation force for parallel polarization well because the self-interaction is much smaller than the separation of exciton levels [see Fig. 2(a)]. However, for perpendicular polarization, this approximation does not provide good agreement with the exact calculation because the self-interaction $\mathrm{Re}(\Delta E_\perp)$ is comparable to the exciton-level separations [see Fig. 2(b)].

Figure 4 shows the dissipative force exerted on SWCNs with diameters of 1.2, 1.4, and 1.6 nm for (a) parallel and (b) perpendicular polarizations. In this figure, we consider SWCNs with a length of 1 μm and an applied field intensity of $I_0=1$ MW/cm^2, which is comparable to that generally used in the optical tweezers.[49] The nonradiative decay width is $\hbar\Gamma=10$ meV, which is the observed luminescence spectral

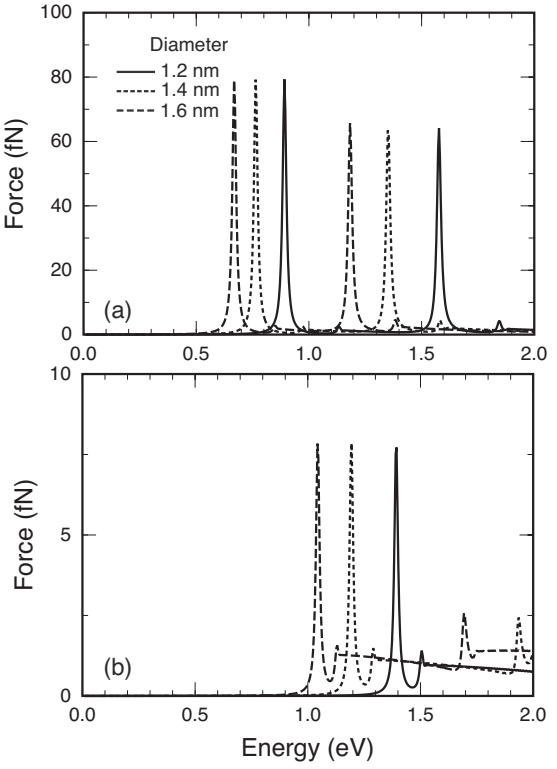

FIG. 4. Calculated dissipative force for an EM field with (a) parallel and (b) perpendicular polarization. Coulomb interaction is set to be $\tilde{v}=0.15$.

width at room temperature.[50–52] At the resonant condition, the force is 80 fN, and the corresponding acceleration is 2.8×10^7 m/s^2, where the mass density of a SWCN is 7.6×10^{-8} g/cm^2. This acceleration is much larger than the gravitational one.

For perpendicular polarization, the peak positions of the dissipative force are different from those for parallel polarization even when the SWCN has the same diameter because of the optical selection rule ($l=0$ for parallel polarization and $l=\pm1$ for perpendicular polarization) and the shift in the depolarization peak for the perpendicular polarization. In addition, the depolarization effect suppresses the force peaks.

A SWCN does not have a rigid structure in the axial direction in standard experimental conditions and is generally twisted in various directions. The above calculations are limited to a SWCN with a straight axis. In order to study the radiation force for the twisted SWCNs, we should calculate the statistical average of the force with respect to the axial direction. When segments of a twisted SWCN have a completely random orientation, the averaged force is given by $F_Z^{\parallel\mathrm{av}}(\omega)=F_Z^{\parallel}(\omega)/2+F_Z^{\perp}(\omega)/2$. The exciton levels for perpendicular polarization are different from those for parallel polarization and the force for perpendicular polarization is much smaller than that for parallel polarization. Therefore, it is feasible to consider exciton resonance for parallel polarization in the selective manipulation and sorting of SWCNs. In the selected SWCNs, the major axial orientation will be parallel to the applied field polarization.

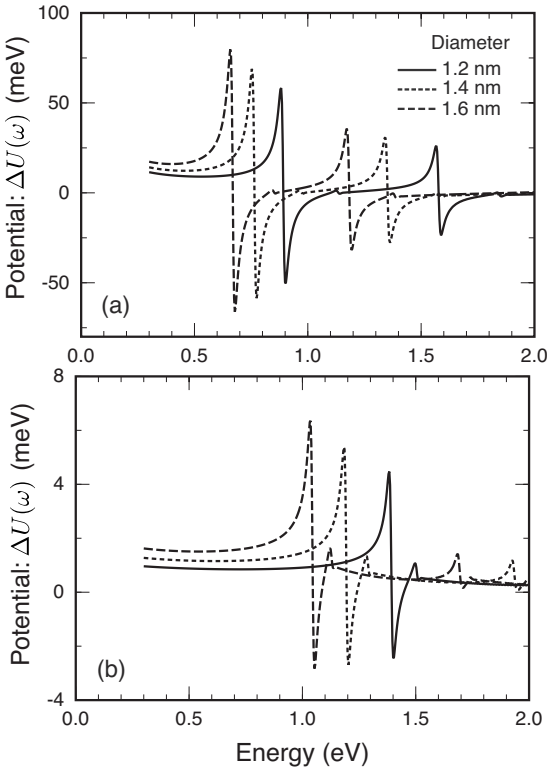

FIG. 5. Calculated potential difference $\Delta U(\omega)$ between minimum and maximum potentials due to a gradient force for an EM field with (a) parallel and (b) perpendicular polarization. Coulomb interaction is set to be $\tilde{v}=0.15$.

B. Gradient force

When the intensity of an EM field has a gradient at an object, a force is exerted on the object. In order to study the gradient force exerted on SWCNs, we consider a standing plane wave consisting of counter-propagating plane waves: $\mathbf{E}_0(\mathbf{r})=2E_0\cos(qZ)\mathbf{e}_{\parallel,\perp}$. We denoted $B_{u,l}^{(0)}$ and $X_{u,l}$ for the standing wave by $B_{u,l}^{(0)\mathrm{st}}$ and $X_{u,l}^{\mathrm{st}}$, respectively. When a SWCN is located at position Z_0, $B_{u,l}^{(0)\mathrm{st}}$ is given by $2\cos(qZ_0)B_{u,l}^{(0)}$ and thus, $X_{u,l}^{\mathrm{st}}=2\cos(qZ_0)X_{u,l}$, where $B_{u,l}^{(0)}$ and $X_{u,l}$ are functions for the traveling wave $\mathbf{E}_0(\mathbf{r})=E_0e^{iqZ}\mathbf{e}_{\parallel,\perp}$. Substituting the above equations into Eq. (28), we obtain the following expression for the gradient force for the standing wave:

$$F_Z(\omega)=f(\omega)\sin(2qZ_0) \tag{36}$$

with

$$f(\omega)=-\frac{\hbar q}{\omega}\mathrm{Re}\left[\sum_{u,l}\frac{1}{E_{u,l}}B_{u,l}^{(0)}X_{u,l}\right]. \tag{37}$$

In the individual-exciton approximation, $f(\omega)$ is written as

$$f(\omega)=-8\kappa_c AI_0\sum_{u,l}\frac{\hbar\Gamma_{\mathrm{rad}}}{E_{u,l}}\frac{\bar{E}_{u,l}-\hbar\omega}{(\bar{E}_{u,l}-\hbar\omega)^2+(\hbar\Gamma+\hbar\Gamma_{\mathrm{rad}})^2}. \tag{38}$$

The gradient force as a function of the applied field frequency exhibits a dispersive line shape and the force is positive or negative depending on the applied field frequency.

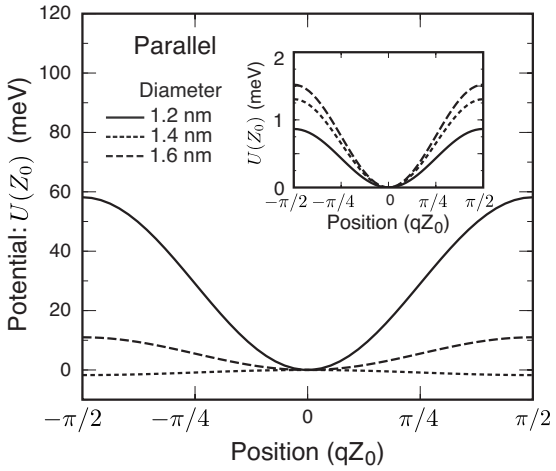

FIG. 6. Calculated potential $U(Z_0)$ due to a gradient force for parallel polarization, shown as a function of SWCN position Z_0. Coulomb interaction is set to be $\tilde{v}=0.15$. The applied field frequency is fixed at $\hbar\omega_0=0.88$ eV, where the SWCN with $d=1.2$ nm experiences the red detuning. The inset shows the potential for perpendicular polarization.

The potential for the gradient force is represented by $U(\omega,Z_0)=f(\omega)[\cos(2qZ_0)-1]/2q$. Minimum or maximum potentials lie at $Z_0=\pi/(2q)+n\pi/q$ or $n\pi/q$ depending on the sign of $f(\omega)$, where n is an integer. The potential difference between minimum and maximum potentials is given by $\Delta U(\omega)=U[\omega,\pi/(2q)]-U(\omega,0)=-f(\omega)/q$. For $f(\omega)>0$ or $\Delta U(\omega)<0$ (blue detuning), potential minima lie at $Z_0=\pi/(2q)+n\pi/q$, where the light intensity is zero. For $f(\omega)<0$ or $\Delta U(\omega)>0$ (red detuning), potential minima lie at $Z_0=n\pi/q$, where the light intensity is maximum.

Figure 5 shows the calculated $\Delta U(\omega)$ for SWCNs with diameters of 1.2, 1.4, and 1.6 nm for (a) parallel and (b) perpendicular polarizations. The length of the SWCN is 1 μm, the intensity of each counter-propagating traveling EM field is $I_0=0.5$ MW/cm^2, and the nonradiative decay width is $\hbar\Gamma=10$ meV. The potential depth reaches 50 meV for parallel polarization and thus, the trapping force on SWCNs can overcome the thermal fluctuation. The potential dips for SWCNs with different diameters are well separated from each other.

Figure 6 shows the potential $U(\omega_0,Z_0)$ for each counter-propagating field intensity $I_0=0.5$ MW/cm^2, where applied field frequency is fixed at $\hbar\omega_0=0.88$ eV. This frequency corresponds to the resonant red detuning for the SWCN with $d=1.2$ nm. The SWCN with $d=1.2$ nm is strongly trapped at the position $Z_0=0$, which is destabilization point for the SWCN with $d=1.4$ nm. An SWCN with $d=1.6$ nm experiences a small potential about 10 meV and thus, the SWCN would move away from the position $Z_0=0$ at room temperature due to the thermal fluctuation. Therefore, only the SWCN with $d=1.2$ nm would be trapped. If we apply stronger laser field such that the potential for the SWCN with $d=1.6$ nm exceeds thermal fluctuation energy, the SWCN with $d=1.6$ nm is also trapped as well as the SWCN with $d=1.2$ nm. From Fig. 5 and the feature that the potential is proportional to the applied field intensity, we can estimate the appropriate laser field intensity for selective trapping of

SWCNs with specific structure. Furthermore, the potential for perpendicular polarization at this position is extremely small (see inset of Fig. 6). This indicates that we can trap SWCNs with the major axial orientation parallel to the light polarization.

V. WARPING EFFECT

In the present approximation scheme, the exciton energy levels depend on the diameter of a SWCN. However, some SWCNs with fairly similar diameters have different chiralities, resulting in different energy gaps for these SWCNs. This feature is clearly observed in a Kataura plot of optical transition energy against diameter, which serves as a common guide for determining the SWCN structure from optical spectra.[53] The chirality dependence of SWCNs with similar diameters mainly originates from the trigonal warping of the energy band of 2D graphite[54] and the finite curvature in the circumference direction.[55,56] The warping effect increases when the energy is away from the Fermi energy and thus, the chirality effect increases with decreasing diameter. The curvature effect causes a shift in the origin for $\hat{k}_x$ and $\hat{k}_y$. The shift in $\hat{k}_x$ is considered as an effective magnetic flux passing through the cross section, i.e., $\Delta k_x=(2\pi/L)(\phi/\phi_0)$,[56] and thus, the band structure is modified by the curvature. Owing to the warping and curvature effects, SWCNs with almost equal diameters have appreciably different exciton energies. As a result, SWCNs with specific chiral vectors can be selectively manipulated and sorted by using the resonant radiation force. Here, we consider warping effect on the radiation force. We do not consider the curvature effect because it is difficult to obtain reliable estimates in the $\mathbf{k}\cdot\mathbf{p}$ treatment. More reliable calculations on exciton states have been performed by utilizing the extended tight-binding model that includes π-σ hybridization due to finite curvature.[57–59]

In the $\mathbf{k}\cdot\mathbf{p}$ scheme, the warping effect can be included by introducing a higher-order $\mathbf{k}\cdot\mathbf{p}$ term. The $\mathbf{k}\cdot\mathbf{p}$ Hamiltonian including higher-order terms around the K point[54] is given by

$$H=\gamma\begin{pmatrix} 0 & \hat{k}_x-i\hat{k}_y+\dfrac{a}{4\sqrt{3}}e^{3i\eta}(\hat{k}_x+i\hat{k}_y)^2 \\ \hat{k}_x+i\hat{k}_y+\dfrac{a}{4\sqrt{3}}e^{-3i\eta}(\hat{k}_x-i\hat{k}_y)^2 & 0 \end{pmatrix}, \tag{39}$$

where η is the chiral angle depicted in Fig. 1(a). The Hamiltonian around the K' point is obtained by taking the complex conjugate and changing η to $\eta+\pi/3$ in Eq. (39). The resulting energy is degenerate around the K and K' points, and the band gaps between optically allowed transitions for parallel polarization are calculated as[38]

$$\kappa_g(n,k)\approx 2\gamma|\kappa_{\nu\varphi}(n)|\left(1+\frac{a\kappa_{\nu\varphi}(n)}{4\sqrt{3}}\cos 3\eta\right). \tag{40}$$

The warping effect does not modify the band gap for armchair SWCNs ($\eta=\pi/6$), while the effect shifts the band gap for zigzag SWCNs ($\eta=0$) by the maximum amount.

Starting from the higher-order effective-mass Hamiltonian, we calculate the radiation force in a similar manner to that in Sec. II. Figure 7 shows the calculated potential due to the gradient force of metallic SWCNs with chiral vectors (19,8), (18,6), and (17,4), which correspond to chiral vectors (11,8), (12,6), and (13,4) for other definitions of primitive translation vectors $\mathbf{a}_1$ and $\mathbf{a}_2$ [see Fig. 1(a)]. These SWCNs have fairly similar diameter and are listed in Ref. 22 as candidates for selectively aggregated SWCNs. Although the diameters of the SWCNs are almost equal, the positions of potential dips for SWCNs with different chiralities are separated from each other because of the warping effect. It is known that the exciton effect enhances the level separation due to the warping and curvature,[59] and the same tendency is observed in Fig. 7. Therefore, by considering the excitonic effect, the resonant radiation force can be effectively used for definite manipulation and sorting of SWCNs with specific structure, even for SWCNs with almost equal diameters.

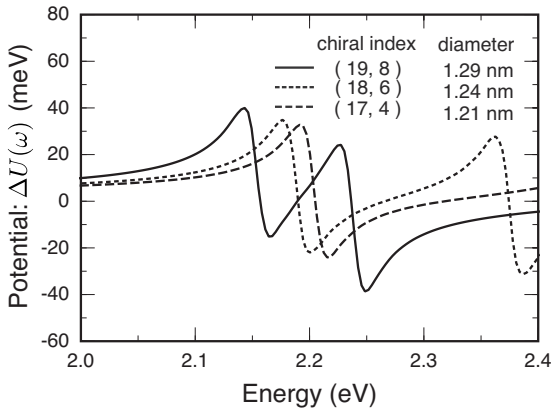

FIG. 7. Potential difference due to the gradient force for parallel polarization. Coulomb interaction is set to be $\tilde{v}=0.15$. The warping effect is included by using a higher-order $\mathbf{k}\cdot\mathbf{p}$ equation. The SWCNs with chiral vectors (19,8), (18,6), and (17,4) are all metallic.

VI. SUMMARY AND CONCLUSION

In summary, we have theoretically studied the radiation force exerted on SWCNs mediated by excitons. The calculation is based on the microscopic optical-response theory, in which the induced current density and total EM field are determined self-consistently. This treatment provides the radiative correction including the radiative shift of the spectral peak and radiative decay line width. Then, the scattering force related to the radiative lifetime can also be obtained by this treatment, and thus, a unified description of absorption and scattering forces becomes possible.

We have calculated the dissipative force for a traveling EM field and the potential of a gradient force for a standing EM field. The applied field polarization is considered to be parallel and perpendicular to the tube axis. The direction of the dissipative force exerted on the SWCN is the same as that of the applied field; the dissipative force consists of absorption and scattering forces. Since the radiative lifetime is very long, the dissipative force is dominated by the absorption force even at low temperatures. In this region, the dissipative force is inversely proportional to the nonradiative decay width.

Both spectra of the dissipative force and the trapping potential due to the gradient force are well separated for SWCNs with different diameters. Even for SWCNs with almost equal diameters, these spectral peaks for SWCNs with different chiralities are separated from each other. Therefore, the selective manipulation and sorting of SWCNs with specific structures is possible by tuning the frequency of the applied EM field. Particularly for the trapping, when we use a linearly polarized standing-wave field, we can trap both low and high intensity regions by applying red- and blue-detuned frequencies, respectively. The resonant frequencies depend on the applied field polarization and the radiation force for perpendicular polarization is much smaller than that for parallel polarization. Although a SWCN does not have rigid structure in the axial direction under standard experimental conditions, these features can be used for optical manipulation and sorting of SWCNs whose major axial orientation is parallel to the applied EM field.

Finally, resonant nano-optical manipulation techniques will enable us to extract and utilize SWCNs with desired diameter, chiralities, and uniform orientation in environment such as vacuum, air, and water at room temperature, which is significantly important in the fundamental and application studies.

ACKNOWLEDGMENTS

This study was supported in part by a Grant-in-Aid for Scientific Research (KAKENHI) under Grants No. 19054013 on Priority Area "Carbon nanotube Nano-Electronics" and No. 19049014 on Priority Area "Strong Photons-Molecules Coupling Fields" from the Ministry of Education, Culture, Sports, Science and Technology (MEXT) of Japan.

*ajiki@ppc.osaka-u.ac.jp

[1] T. Ando, J. Phys. Soc. Jpn. **74**, 777 (2005).
[2] J. C. Charlier, X. Blase, and S. Roche, Rev. Mod. Phys. **79**, 677 (2007).
[3] J. W. Mintmire, B. I. Dunlap, and C. T. White, Phys. Rev. Lett. **68**, 631 (1992).
[4] N. Hamada, S. I. Sawada, and A. Oshiyama, Phys. Rev. Lett. **68**, 1579 (1992).
[5] R. Saito, M. Fujita, G. Dresselhaus, and M. S. Dresselhaus, Phys. Rev. B **46**, 1804 (1992).
[6] H. Ajiki and T. Ando, J. Phys. Soc. Jpn. **62**, 1255 (1993).
[7] S. Zaric, G. N. Ostojic, J. Kono, J. Shaver, V. C. Moore, M. S. Strano, R. H. Hauge, R. E. Smalley, and X. Wei, Science **304**, 1129 (2004).
[8] R. Matsunaga, K. Matsuda, and Y. Kanemitsu, Phys. Rev. Lett. **101**, 147404 (2008).
[9] L. Nilsson, O. Groening, C. Emmenegger, O. Kuettel, E. Shaller, L. Schlapbach, H. Kind, J.-M. Bonard, and K. Kern, Appl. Phys. Lett. **76**, 2071 (2000).
[10] S. Akita, H. Nishijima, Y. Nakayama, F. Tokumasu, and K. Takeyasu, J. Phys. D **32**, 1044 (1999).
[11] D. Mann, Y. K. Kato, A. Kinkhabwala, E. Pop, J. Cao, X. Wang, L. Zhang, Q. Wang, J. Guo, and H. Dai, Nat. Nanotechnol. **2**, 33 (2007).
[12] A. Javey, J. Guo, Q. Wang, M. Lundstrom, and H. J. Dai, Nature (London) **424**, 654 (2003).
[13] A. Kojima, C. K. Hyon, T. Kamimura, M. Maeda, and K. Matsumoto, Jpn. J. Appl. Phys. **44**, 1596 (2005).
[14] A. Jorio, M. S. Dresselhaus, and G. Dresselhaus, *Carbon Nanotubes: Advanced Topics in the Synthesis, Structure, Properties and Applications* (Springer-Verlag, Berlin, 2008).
[15] T. Iida and H. Ishihara, Phys. Rev. Lett. **90**, 057403 (2003).
[16] T. Iida and H. Ishihara, IEICE Trans. Electron. **E88-C**, 1809 (2005).
[17] T. Iida and H. Ishihara, Phys. Rev. B **77**, 245319 (2008).
[18] K. Inaba, K. Imaizumi, K. Katayama, M. Ichimiya, M. Ashida, T. Iida, H. Ishihara, and T. Itoh, Phys. Status Solidi B **243**, 3829 (2006).
[19] C. Hosokawa, H. Yoshikawa, and H. Masuhara, Jpn. J. Appl. Phys., Part 2 **45**, L453 (2006).
[20] H. Li, D. Zhou, H. Browne, and D. Klenerman, J. Am. Chem. Soc. **128**, 5711 (2006).
[21] S. Tan, H. A. Lopez, C. W. Cai, and Y. Zhang, Nano Lett. **4**, 1415 (2004).
[22] T. Rodgers, S. Shoji, Z. Sekkat, and S. Kawata, Phys. Rev. Lett. **101**, 127402 (2008).
[23] H. Ajiki, T. Ishikawa, T. Iida, and H. Ishihara, Phys. Status Solidi C **6**, 65 (2009).
[24] T. Ando, J. Phys. Soc. Jpn. **75**, 024707 (2006).
[25] T. Iida and H. Ishihara, Phys. Rev. Lett. **97**, 117402 (2006).
[26] K. Cho, *Optical Response of Nanostructures* (Springer, Berlin, 2003).
[27] H. Ajiki and T. Ando, Physica B **201**, 349 (1994).
[28] H. Ajiki, Phys. Rev. B **65**, 233409 (2002).

[29] T. Ando, J. Phys. Soc. Jpn. **66**, 1066 (1997).
[30] M. Ichida, S. Mizuno, Y. Tani, Y. Saito, and A. Nakamura, J. Phys. Soc. Jpn. **68**, 3131 (1999).
[31] M. Ichida, S. Mizuno, Y. Saito, H. Kataura, Y. Achiba, and A. Nakamura, Phys. Rev. B **65**, 241407(R) (2002).
[32] S. M. Bachilo, M. S. Strano, C. Kittrell, R. H. Hauge, R. E. Smalley, and R. B. Weisman, Science **298**, 2361 (2002).
[33] A. Hagen and T. Hertel, Nano Lett. **3**, 383 (2003).
[34] M. J. O'Connell, S. M. Bachilo, C. B. Huffman, V. C. Moore, M. S. Strano, E. H. Haroz, K. L. Rialon, P. J. Boul, W. H. Noon, C. Kittrell, J. Ma, R. H. Hauge, R. B. Weisman, and R. E. Smalley, Science **297**, 593 (2002).
[35] S. Lebedkin, K. Arnold, F. Hennrich, R. Krupke, B. Renker, and M. M. Kapes, New J. Phys. **5**, 140 (2003).
[36] S. Uryu and T. Ando, Phys. Rev. B **74**, 155411 (2006).
[37] S. Uryu, H. Ajiki, and T. Ando, Phys. Rev. B **78**, 115414 (2008).
[38] T. Ando, J. Phys. Soc. Jpn. **73**, 3351 (2004).
[39] H. Ajiki and T. Ando, J. Phys. Soc. Jpn. **62**, 2470 (1993); **63**, 4267(E) (1994).
[40] N. A. Viet, H. Ajiki, and T. Ando, J. Phys. Soc. Jpn. **63**, 3036 (1994).
[41] H. Suzuura and T. Ando, in *Proceedings of the 25th International Conference on Physics of Semiconductors*, edited by N. Miura and T. Ando (Springer, Berlin, 2001), p. 1525.
[42] K. Cho, Prog. Theor. Phys. **106**, 225 (1991).
[43] H. Ajiki, T. Tsuji, K. Kawano, and K. Cho, Phys. Rev. B **66**, 245322 (2002).
[44] W. Chew, *Waves and Fields in Inhomogeneous Media* (IEEE, Piscataway, New Jersey, 1995).
[45] C. D. Spataru, S. Ismail-Beigi, R. B. Capaz, and S. G. Louie, Phys. Rev. Lett. **95**, 247402 (2005).
[46] D. S. Citrin, Phys. Rev. Lett. **69**, 3393 (1992).
[47] A. Hagen, G. Moos, V. Talalaev, and T. Hertel, Appl. Phys. A: Mater. Sci. Process. **78**, 1137 (2004).
[48] A. Ashkin, J. M. Dziedzic, J. E. Bjorkholm, and S. Chu, Opt. Lett. **11**, 288 (1986).
[49] H. J. Guntherodt, D. Anselmetti, and E. Meyer, in *Forces in Scanning Probe Methods*, NATO Advanced Studies Institute, Series B: Physics (Kluwer Academic, Dordrecht, 1995).
[50] T. Inoue, K. Matsuda, Y. Murakami, S. Maruyama, and Y. Kanemitsu, Phys. Rev. B **73**, 233401 (2006).
[51] K. Matsuda, T. Inoue, Y. Murakami, S. Maruyama, and Y. Kanemitsu, Phys. Rev. B **77**, 033406 (2008).
[52] M. Ichida, Y. Kiyohara, S. Saito, Y. Miyata, H. Kataura, and H. Ando, Phys. Status Solidi B **245**, 2712 (2008).
[53] H. Kataura, Y. Kumazawa, Y. Maniwa, I. Umezu, S. Suzuki, Y. Ohtsuka, and Y. Achiba, Synth. Met. **103**, 2555 (1999).
[54] H. Ajiki and T. Ando, J. Phys. Soc. Jpn. **65**, 505 (1996).
[55] X. Blase, L. X. Benedict, E. L. Shirley, and S. G. Louie, Phys. Rev. Lett. **72**, 1878 (1994).
[56] T. Ando, J. Phys. Soc. Jpn. **69**, 1757 (2000).
[57] V. N. Popov, New J. Phys. **6**, 17 (2004).
[58] G. G. Samsonidze, R. Saito, N. Kobayashi, A. Gröneis, J. Jiang, A. Jorio, S. G. Chou, G. Dresselhaus, and M. S. Dresselhaus, Appl. Phys. Lett. **85**, 5703 (2004).
[59] J. Jiang, R. Saito, G. G. Samsonidze, A. Jorio, S. G. Chou, G. Dresselhaus, and M. S. Dresselhaus, Phys. Rev. B **75**, 035407 (2007).